Journal of Power Sources 196 (2011) 2848–2853

Contents lists available at ScienceDirect

Journal of Power Sources

journal homepage: www.elsevier.com/locate/jpowsour

Structural transformation of layered hydrogen trititanate ($H_2Ti_3O_7$) to TiO_2(B) and its electrochemical profile for lithium-ion intercalation

Guan-Nan Zhu, Cong-Xiao Wang, Yong-Yao Xia*

Department of Chemistry and Shanghai Key Laboratory of Molecular Catalysis and Innovative Materials, Institute of New Energy, Fudan University, Handan Rd. 220, Shanghai 200433, China

ARTICLE INFO

Article history:
Received 16 March 2010
Received in revised form 1 July 2010
Accepted 8 July 2010
Available online 15 July 2010

Keywords:
Lithium titanates
Hydrogen titanates
Thermal transformation
Lithium-ion batteries

ABSTRACT

The thermally-induced structural transformation of layered hydrogen trititanate ($H_2Ti_3O_7$) to TiO_2(B) has been systematically studied by means of in situ X-ray diffraction (XRD) over a wide temperature range from 170 to 450 °C. Our data indicate a structural transition realized via continuous loss of interlayer water, which results in a series of non-stoichiometric hydrogen titanate compounds ($3TiO_2{\cdot}\delta H_2O$). Electrochemical analysis of hydrogen titanates for lithium-ion intercalation shows that reversible specific capacity increases as calcination temperature increases, whereas cycling stability decreases during the continuous dehydration process.

1. Introduction

A monoclinic layered hydrogen trititanate ($H_2Ti_3O_7$), consisting of negatively charged layered sheets of corner- and edge-shared TiO_6 octahedra [1] and protons in the interlayer, has been synthesized by proton exchange of alkalimetal titanates $A_2Ti_3O_7$ [1–4] (A = Na, Li, K etc.) which could be prepared either by solid state reaction or hydrothermal treatment. This titanate, initially discovered as an intermediate of fabricating TiO_2(B) by hydrothermal treatment, has developed strong potential for applications in various fields. As an n-type semiconductor, hydrogen trititanate often shows excellent photocatalytic activity [1,5,6]. Riss [7] explored the photoelectronic properties of $H_2Ti_3O_7$ nanotubes, indicating that the chemical composition, structure and condition of the interface play decisive roles in photocatalytic activity. Hydrogen trititanate could also be used in fuel cells [8,9] to achieve high proton conductivity.

Recently, much attention has been given to this material as an ideal host for lithium-ion intercalation due to its layered structure [10]. Li et al. [9,11] prepared hydrogen trititanate $H_2Ti_3O_7$ nanowires and nanotubes; they reported that these materials deliver electrochemical capacity as high as 330 mAh g^{-1} and excellent rate performance. In addition, $H_2Ti_3O_7$ may be converted into TiO_2(B) via multistep transformation occurring between 120 and 400 °C through topotactic mechanisms with the intermediate formation of $H_2Ti_6O_{13}$ and $H_2Ti_{12}O_{25}$ [2]. The TiO_2(B) with different morphologies prepared by thermal transformation as described above (e.g., nanowires [12–14] or nanotubes [15–18]) also exhibits good electrochemical performance for lithium-ion intercalation. However, the thermal transformation of $H_2Ti_3O_7$ to TiO_2(B) has not been studied in detail, and the electrochemical profile of the occurring intermediate compounds has not been addressed.

In the present work, we investigate the thermal transformation of $H_2Ti_3O_7$ by means of in situ and ex situ XRD and thermogravimetric analysis (TGA). The phase and chemical composition of $H_xTi_yO_z$ with different ratios of H, Ti and O as a function of temperature were systematically studied. Furthermore, the electrochemical performance for lithium-ion intercalation of as-synthesized and heat-treated $H_2Ti_3O_7$ were measured and compared.

2. Experimental

2.1. Synthesis of $H_2Ti_3O_7$

The precursor $Na_2Ti_3O_7$ was prepared according to a previously reported procedure [19]. A mixture of stoichiometric quantities of dried Na_2CO_3 and TiO_2 (anatase) (1:3 molar ratio) was realized by wet-ball-milling using a Pulverisette 6 (Fritsch Gmbh.In., Germany) with ethanol as a dispersing agent and a weight ratio of agate ball-to-powder of 10:1 for 6 h. The slurry was then dried and calcined at 800 °C for 20 h in air. The resultant $Na_2Ti_3O_7$ powder subsequently underwent acid exchange in 500 mL 0.1 M HCl under magnetic agitation at room temperature for 5 days. The acid solution was renewed every 24 h in order to completely remove the

* Corresponding author. Tel.: +86 21 51630318; fax: +86 21 51630318.
E-mail address: yyxia@fudan.edu.cn (Y.-Y. Xia).

0378-7753/$ – see front matter © 2010 Elsevier B.V. All rights reserved.
doi:10.1016/j.jpowsour.2010.07.023

alkali from the compound. The product was finally washed with deionized water and dried overnight at 120 °C.

2.2. Thermal transformation of $H_2Ti_3O_7$ by in situ XRD and TG tests

The as-synthesized $H_2Ti_3O_7$ was analyzed by in situ high-temperature X-ray diffraction (HT-XRD) at 170, 200, 230, 260, 290, 320, 350, 380, 410 and 450 °C using a Bruker Advance 8 X-ray diffractometor. Each XRD pattern was recorded at a scanning rate of 1.7° min^{-1} from $2\theta = 10°$ to 30°. Thermogravimetric analysis (TGA) of $H_2Ti_3O_7$ was conducted by increasing temperature from 25 to 500 °C at a heating rate of 1 °C min^{-1} with Ar flow of 50 mL min^{-1} with a Perkin-Elmer TGA 7 thermal analyzer.

2.3. Weight loss experiment by heat treatment of $H_2Ti_3O_7$

The phase and chemical composition of the intermediate compounds were studied by ex situ XRD tests and weight loss experiments. The as-synthesized $H_2Ti_3O_7$ was first vacuum-dried at 100 °C for 5 h to remove adsorbed water; exactly 5 g of this compound was heat-treated at a rate of 1 °C min^{-1} to a set temperature (155, 170, 200, 230, 240, 250, 260, 270, 320, 350, 370, 380, 390, 400, 410 and 450 °C, respectively) and held at that temperature for 6 h, cooled, and massed again. The mass of lost water Δm was calculated by the mass difference of the sample before and after heat treatment. The resulting compounds were also characterized by ex situ XRD at a scanning rate of 5° min^{-1} from $2\theta = 10°$ to 90°.

2.4. Characterization of heat-treated samples of $H_2Ti_3O_7$

The morphologies of three typical heat-treated samples were characterized by a Joel JSM6390 scanning electron microscope and a Joel JEM2010 transmission electron microscope, respectively.

2.5. Electrochemical tests for as-synthesized and heat-treated $H_2Ti_3O_7$

For electrochemical tests, composite working electrodes of the as-synthesized and heat-treated samples were prepared by mixing 90 wt% active material, 5 wt% carbon black, and 5 wt% poly(tetrafluoroethylene) (PTFE) dispersed in isopropanol. The slurry was cast on a steel current collector and dried at 80 °C for 10 min to remove the solvent before pressing. Electrode disks were then punched with a diameter of 12 mm and 5 mg cm^{-2} typical mass load of active material. The composite electrodes were dried at 120 °C for 12 h before assembling. Coin-type cells (CR2016) were assembled as positive electrode (working electrode)/separator/negative electrode (lithium metal) layers using an electrolyte solution of 1 M $LiPF_6$, ethylene carbonate (EC), dimethyl carbonate (DMC), and methyl carbonate (1:1:1 by volume) in an argon-filled glove box. The electrochemical performance of the half cells was evaluated with a battery test system (LAND CT2001A, Wuhan Jinnuo Electronics Co., Ltd.).

3. Results and discussion

3.1. Characterization of $Na_2Ti_3O_7$ and $H_2Ti_3O_7$

Fig. 1 shows typical XRD patterns of $Na_2Ti_3O_7$ and $H_2Ti_3O_7$. $H_2Ti_3O_7$ was obtained by acid treatment of $Na_2Ti_3O_7$ and subsequent drying at 120 °C; inductively coupled plasma (ICP) analysis revealed no residual Na. Both $Na_2Ti_3O_7$ and $H_2Ti_3O_7$ were determined to be phase-pure based on their XRD patterns. The X-ray diffraction peaks for $H_2Ti_3O_7$ can be indexed as monoclinic with the following cell parameters: $a = 16.028$ Å, $b = 3.751$ Å, $c = 9.193$ Å and $\beta = 101.6°$. These results agree well with previous crystallographic data for this compound [20].

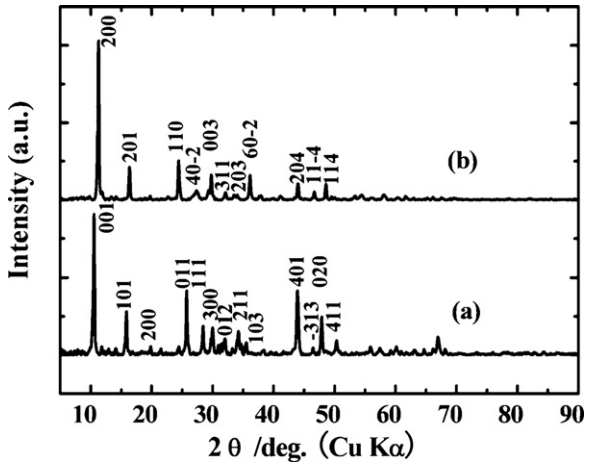

Fig. 1. Typical XRD patterns of (a) $Na_2Ti_3O_7$ and (b) as-synthesized $H_2Ti_3O_7$.

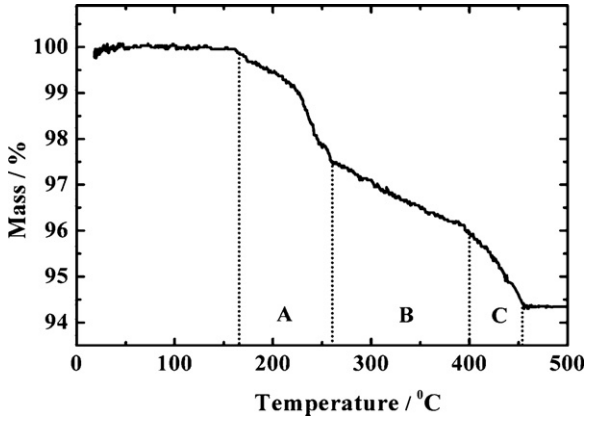

Fig. 2. TGA curve of the as-synthesized $H_2Ti_3O_7$ in Ar flow from 25 °C to 500 °C at a heating rate of 1 °C min^{-1}.

Fig. 2 gives the TGA curve of $H_2Ti_3O_7$ from 25 to 500 °C to initially investigate the thermal transformation process of $H_2Ti_3O_7$ to

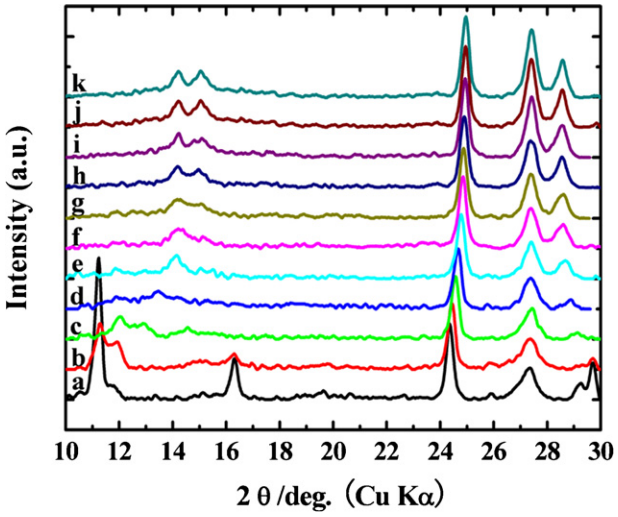

Fig. 3. In situ XRD patterns of as-synthesized $H_2Ti_3O_7$ at different temperatures between 140 °C and 450 °C: (a) 140 °C, (b) 170 °C, (c) 200 °C, (d) 230 °C, (e) 260 °C, (f) 290 °C, (g) 320 °C, (h) 350 °C, (i) 380 °C, (j) 410 °C, and (k) 450 °C. Each XRD pattern was recorded at a scanning rate of 1.7° min^{-1} from $2\theta = 10°$ to 30°.

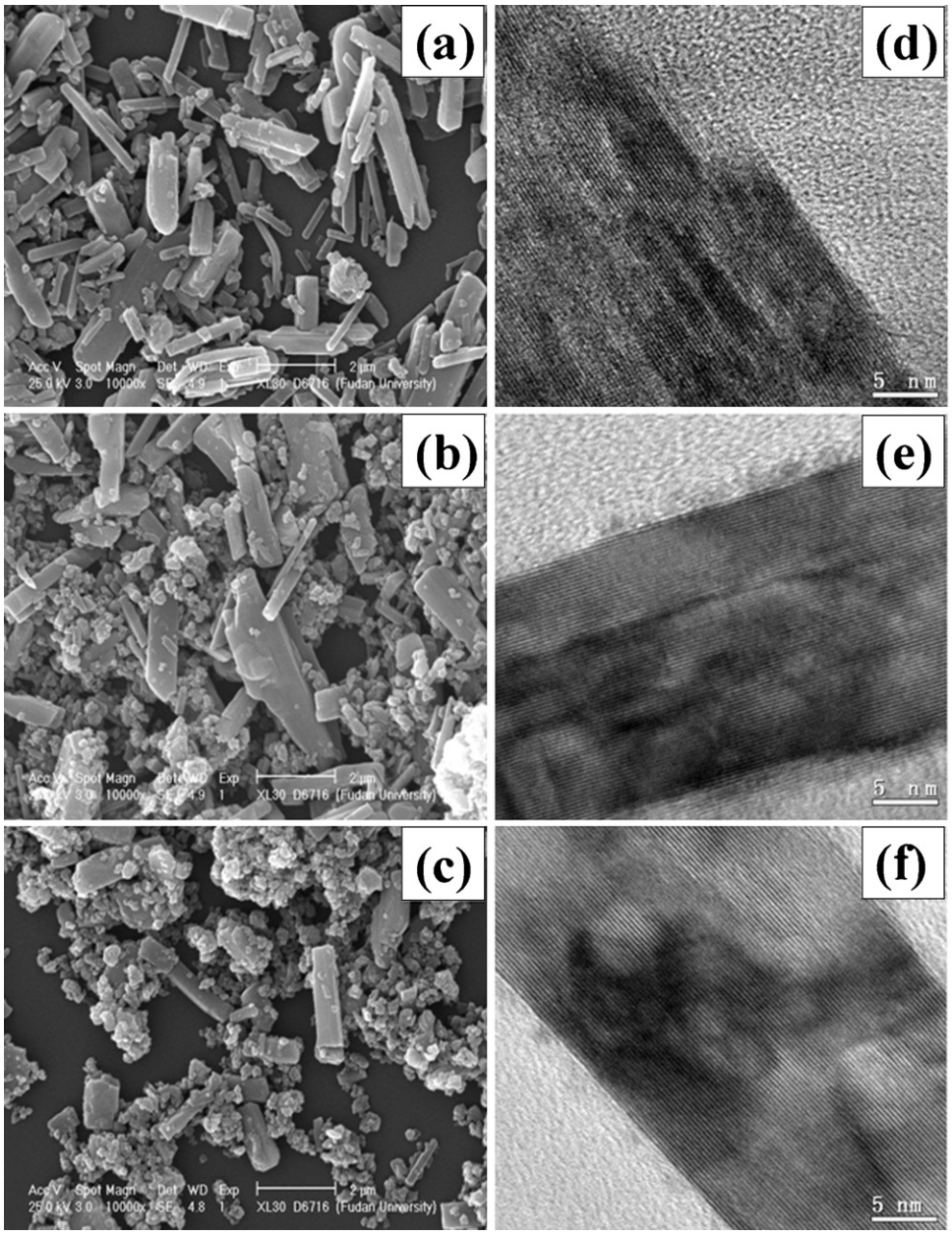

Fig. 4. SEM images for three typical heat-treated samples obtained by calcination of $H_2Ti_3O_7$ for 6 h at (a) 170 °C, (b) 320 °C, and (c) 450 °C; TEM images for the three samples treated at (d) 170 °C, (e) 320 °C, and (f) 450 °C.

TiO_2(B). Water weight loss begins at about 170 °C. Three regions with different water loss rates indicated by different slopes in TGA curve were detected, suggesting the thermal phase transformation undergoes three different processes in the regions between 160 and 260 °C, 260 and 400 °C, and 400 and 450 °C (denoted as regions A, B and C, respectively). Almost no plateaus in the TGA curves were observed at either region, revealing that the process of water loss process was continuous. When the temperature was increased to 450 °C, the total weight loss was about 6% – approximate to the theoretical weight loss of $H_2Ti_3O_7$ to TiO_2(B) (6.8%) and no further weight loss was detected.

3.2. Thermal transformation analysis

The thermally-induced structural transformation of layered hydrogen trititanate $H_2Ti_3O_7$ to TiO_2(B) was further investigated by in situ XRD from 140 to 450 °C. Fig. 3 shows the selected XRD patterns from $2\theta = 10°$ to 30°, in which the diffraction intensity is relatively strong. When the temperature was increased from 140 to 230 °C, corresponding to Region A in Fig. 2, the peak assigned as (2 0 1) gradually disappeared, and the (2 0 0) peaks at $2\theta = 11°$ shifted to larger angles, indicating a gradual reduction of the interlayer distance d_{200} to form a more condensed structure. When the temperature was increased further, corresponding to Region B in Fig. 2, the (2 0 0) and (2 0 1) peaks disappeared completely, whereas three new peaks at $2\theta = 14°$, 15°, and 28.6° were observed. Throughout the whole water loss process, the (1 1 0) peak at $2\theta = 24°$ shifted to larger angles continuously. The above findings strongly indicate the resulting compounds in Regions A–C of Fig. 2 exhibit more condensed structures with increasing temperature.

A series of heat-treated samples was obtained by annealing the as-synthesized $H_2Ti_3O_7$ for 6 h under different temperatures from 170 to 450 °C. Fig. 4(a–c) shows SEM images of three typical heat-treated samples for different temperatures. From Fig. 4(a),

the 170 °C – treated sample has a needle-like structure with a diameter of ca. 400 nm and a length of ca. 2 μm. With the calcination temperature increases to 320 and 450 °C (Fig. 4(b) and (c)), the needle-like shape collapses gradually and is partially replaced by large particle morphology of an average size of ca. 1 μm with agglomerates of small crystallites on the surface, indicating that a higher temperature can promote the contraction of materials. The corresponding TEM images for the three heat-treated samples are shown in Fig. 4(d–f). They all show a clear layered structure, suggesting such structure could be maintained throughout the process of thermal transformation. Additionally, the phase compositions of different heat-treated samples were studied by the ex situ XRD patterns and illustrated in Fig. 5. The results show good agreement with the in situ XRD patterns (Fig. 3) under corresponding temperature, suggesting that these intermediates exist thermodynamically stable.

Based on these results, we hypothesize that the precursor $H_2Ti_3O_7$ undergoes a continuous thermal transformation accompanied by formation of different intermediates, which we attribute to the loss of interlayer water. In fact, such spontaneous rearrangement from one form to the other can easily occur and is expected to be driven by changes in the local water partial pressure [21]. This conclusion is supported by the findings of Wadsley and Anderson, [22,23] who introduced "block-structure theory" and "intergrowth policy" whereby sodium titanates are presented as a series of homologues consisting of numerous blocks whose stoichiometry (Na/Ti/O) can be adjusted by altering block size or intergrowth of several existing separate block structures. Several typical compounds with different blocks marked by black rectangular areas are illustrated in Fig. 6, which support these findings. Due to the structural similarity between sodium titanates and hydrogen titanates, [1–3] the mechanism of thermal transformation may

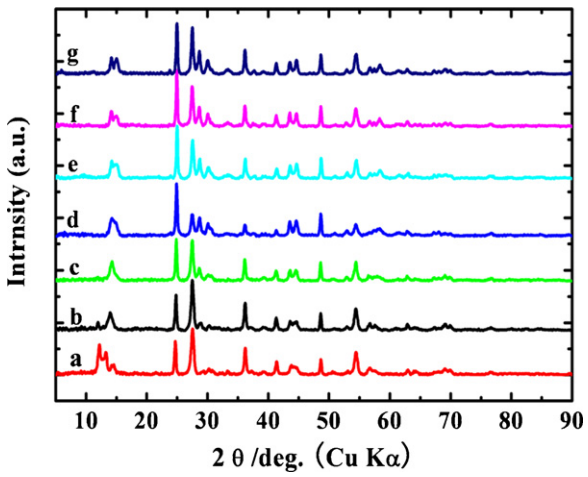

Fig. 5. Ex situ XRD patterns of heat-treated samples under different temperatures: (a) 170 °C, (b) 230 °C, (c) 260 °C, (d) 320 °C, (e) 350 °C, (f) 380 °C, and (g) 450 °C.

be explained by the supposition that $H_2Ti_3O_7$ experiences a similar structural transformation path from (a) to (e) (Fig. 6); During this transformation path, a series of intermediates are formed, each of which can be denoted in standard layered notation as $H_xTi_yO_z$.

Weight loss experiments were carried out to identify the relationship between temperature and chemical composition of $H_xTi_yO_z$ intermediates, which could be reformulated in two-component notation as $3TiO_2{\cdot}\delta H_2O$ $(0 \le \delta \le 1)$ and "δ" was determined from the mass of dehydration Δm by $\delta = 859/300 \times \Delta m$. Based on the experimental and calculated

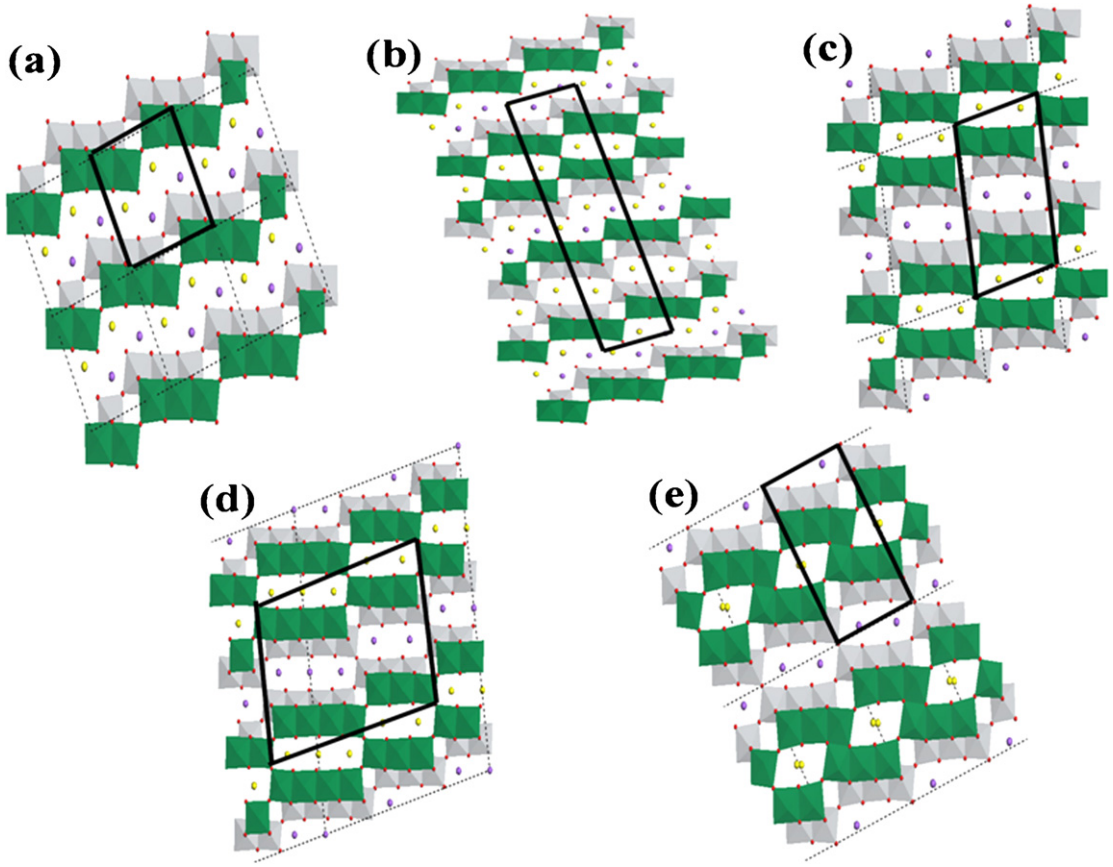

Fig. 6. The structures of (a) $Na_2Ti_3O_7$, (b) $Na_6Ti_{12}O_{27}$, (c) $Na_2Ti_6O_{13}$, (d) $Na_2Ti_7O_{15}$ and (e) $Na_2Ti_{12}O_{25}$ with block sizes of (2×2), (3×4), (3×2), (7×2), and (4×2), respectively.

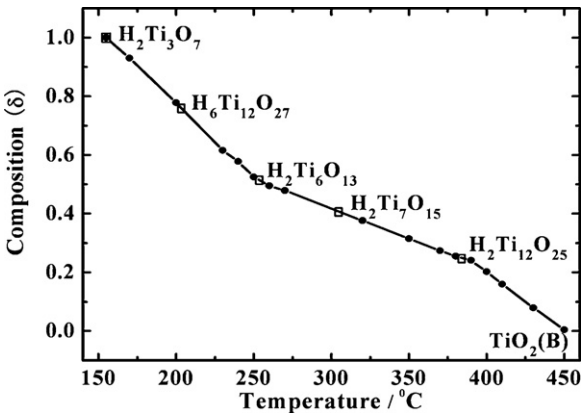

Fig. 7. Composition (δ in $3TiO_2{\cdot}\delta H_2O$) as a function of temperature during thermal transformation of the as-synthesized $H_2Ti_3O_7$ to TiO_2(B). Several hydrogen titanates corresponding to reported sodium titanates [20] in Fig. 5 are labeled as "□".

results, Fig. 7 shows the correlation between chemical composition and temperature. In particular, several non-stoichiometric compounds with structures similar to reported alkalimetal titanates [22] (Fig. 6) are labeled: $H_2Ti_3O_7$ ($3TiO_2{\cdot}1H_2O$), $H_6Ti_{12}O_{27}$ ($3TiO_2{\cdot}0.75H_2O$), $H_2Ti_6O_{13}$ ($3TiO_2{\cdot}0.5H_2O$), $H_2Ti_7O_{15}$ ($3TiO_2{\cdot}0.43H_2O$) and $H_2Ti_{12}O_{25}$ ($3TiO_2{\cdot}0.25H_2O$). Consecutive release of 52%, 26%, and 24% of the total water content can be inferred to correspond to the three thermogravimetric regions of 160–260 °C, 260–400 °C, and 400–450 °C, which agrees well with TGA results in Fig. 2. Moreover, this roughly-estimated proportion of ~2:1:1 in the sequence of released water corresponds to two intermediates of $H_2Ti_6O_{13}$ and $H_2Ti_{12}O_{25}$ at about 258 and 382 °C, and the final product of TiO_2(B) at 450 °C, also consistent with the transformation path previously reported [2]. On the one hand, the three zones display good linearity, indicating that dehydration takes place at constant rates for each respective region. On the other hand, two "transition" areas of 230–270 °C and 350–410 °C connecting neighboring zones are characterized by larger fluctuations, suggesting the occurrence of dramatic changes in dehydration rate. It is likely that the distinct dehydration rate is attributed to the different energies required to form new crystal lattices by different mechanisms (either altering the block size or intergrowth of existing blocks) [22].

The results in Fig. 7 also elucidate the data from in and ex situ XRD (Figs. 3 and 5). For example, peak shifts and intensity changes beginning at 230 and 350 °C in XRD patterns indicate significant structural transformation at these temperatures. In addition, these temperatures correspond with excellent agreement to the "transition" regions depicted in Fig. 7. Finally, these data correspond as well to previously reported transformations from the original "open" structure of $H_2Ti_3O_7$ to "cage" and "tunnel" structures at 258 and 382 °C, respectively [2]. The changes revealed by XRD could therefore be attributed to the formation of new structures.

3.3. Electrochemical performances of different intermediates ($3TiO_2{\cdot}\delta H_2O$)

Titanates are ideal hosts for lithium-ion intercalation due to their layered structures. This may be attributed to the interspaces in the layered titanates, which provide short diffusion distances to facilitate Li ion insertion/extraction [10]. The electrochemical properties of a series of $3TiO_2{\cdot}\delta H_2O$ ($0 \le \delta \le 1$) were evaluated as electrode materials for lithium-ion intercalation.

Fig. 8 reflects the typical discharge–charge curves for an electrode composed of $H_2Ti_3O_7$ (150 °C, a), $3TiO_2{\cdot}0.3778H_2O$ (320 °C, b), and TiO_2(B) (450 °C, c). The profiles of the three selected samples clearly exhibit a sloped feature, indicating that the electrochemical reaction and lithium intercalation remains a single-phase process without the formation of a biphasic interface [24].

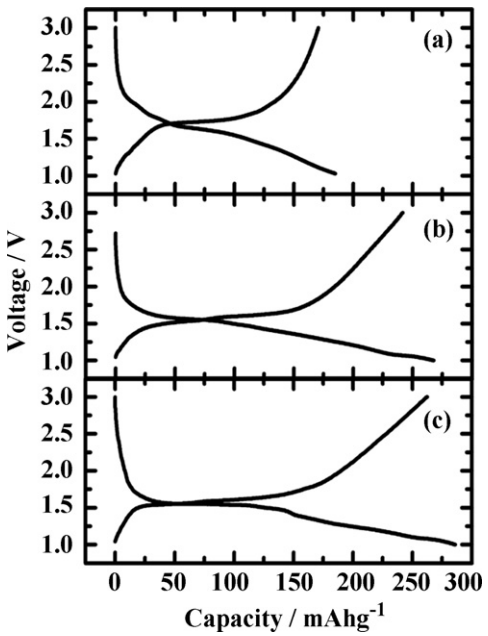

Fig. 8. Typical charge/discharge curves of (a) $H_2Ti_3O_7$ (150 °C), (b) $3TiO_2{\cdot}0.3778H_2O$ (320 °C), and (c) TiO_2(B) (450 °C) between 1.0 V and 3.0 V at a rate of 0.1 Ag^{-1}.

As Fig. 9 shows, with water content δ decreases, the initial discharge capacity increases from 191 mAh g^{-1} ($H_2Ti_3O_7$, $\delta = 1$) to 291 mAh g^{-1} (TiO_2(B), $\delta = 0$). The initial discharge capacity is thus demonstrated to be directly related to the content of the electrochemically active component of TiO_2 in $3TiO_2{\cdot}\delta H_2O$.

A comparison of initial coulombic efficiency between different samples is given in Fig. 9, where it is shown that as δ in $3TiO_2{\cdot}\delta H_2O$ decreases, coulombic efficiency increases from 89% for $H_2Ti_3O_7$, to 92% for TiO_2(B). It has been demonstrated that the shift among layers as well as changes in interlayer distance upon lithium-ion intercalation may make this electrochemical irreversibility inevitable in materials of layered structure [10]. The improved coulombic efficiency is attributed to continuous formation of more condensed structures as indicated in Figs. 3 and 5. Compared to its less-hydrated intermediates, the larger interlayer spacing (and hence, less condensed structure) of $H_2Ti_3O_7$ promotes relaxation

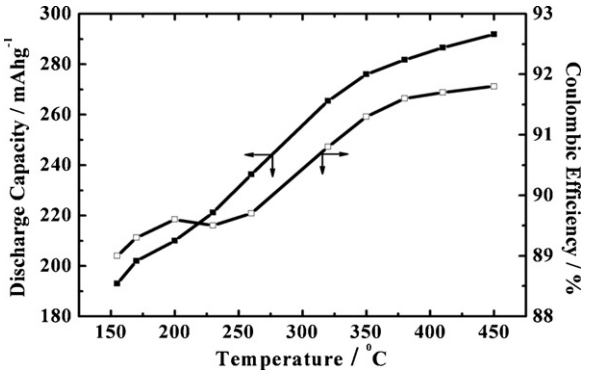

Fig. 9. Initial discharge capacity and coulombic efficiency vs. temperature. The cell was charged/discharged at a rate of 0.1 Ag^{-1} between 1.0 V and 3.0 V.

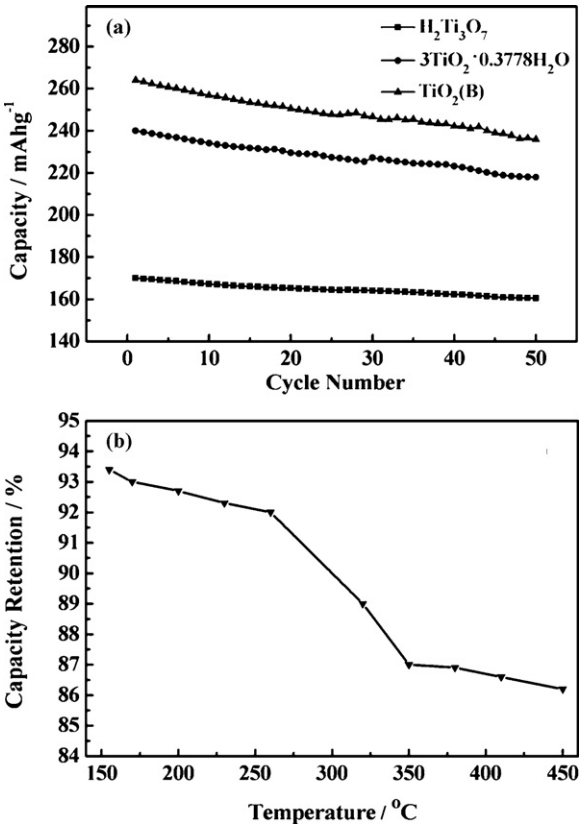

Fig. 10. (a) Cycling performance of three typical heat-treated samples: $H_2Ti_3O_7$, $3TiO_2 \cdot 0.3778H_2O$ and TiO_2(B); (b) the capacity retention (charge capacity of 50th vs. 1st cycle) as a function of temperature. All the electrodes were cycled at a rate of 0.1 Ag^{-1} between 1.0 V and 3.0 V.

and shift among layers, making it more suitable for trapping of Li^+ ions [12]. Furthermore, water incorporated within the crystal structure could react irreversibly with metallic lithium to form Li_2O within the interlayer or on the crystal surface [10]. Taking this possibility into consideration, during the thermal transformation of $H_2Ti_3O_7$, intermediates containing less crystal water would show better initial reversibility, which is consistent with our findings.

The cycling stability of three selected samples, $H_2Ti_3O_7$ (150 °C), $3TiO_2$ $0.3778H_2O$ (320 °C), and TiO_2(B) (450 °C), is shown in Fig. 10(a). They all display rapid capacity fading (>5%) during the initial 10 cycles and less pronounced fading in subsequent cycles. Note that the intermediate with a smaller value of δ exhibits poor cycling stability (Fig. 10(b)), which is primarily due to structural change during heat treatment. The larger interlayer spacing in $H_2Ti_3O_7$, despite its disadvantage of giving rise to greater structural variation upon initial lithium-ion intercalation, provides a broad 1D diffusion pathway along which Li ions undergo more facile transport, better accommodating structural strain during subsequent cycles [12]. In contrast, the sample with a more condensed structure displays superior discharge capacity and initial coulombic efficiency, but inferior cycling stability.

4. Conclusions

We have shown that as-synthesized $H_2Ti_3O_7$ rearranges into TiO_2(B) by heating via a continuous process of water loss accompanied by formation of numerous intermediates. This process can be divided into three distinct areas with different dehydration rates, which correspond to a typical transformation from an "open" structure to a "cage" and finally a "tunnel" structure. Both the weight loss and ex situ XRD experiments indicate that the thermal transformation gives rise to a series of non-stoichiometric hydrogen titanate compounds denoted as $3TiO_2 \cdot \delta H_2O (0 \le \delta \le 1)$, and these compounds could exist thermodynamically. Electrochemical tests reveal that with a decrease of water content δ in $3TiO_2 \cdot \delta H_2O$, the initial discharge capacity increases from 193 of $H_2Ti_3O_7$ ($\delta = 1$) to 291 mAh g^{-1} of TiO_2(B) ($\delta = 0$), and the initial coulombic efficiency is enhanced from 89% to 93%, whereas the cycling stability reflected by the capacity retention (charge capacity of 50th vs. 1st cycle) decreases from 93% of $H_2Ti_3O_7$ to 87% of TiO_2(B). This initial enhancement in capacity and subsequent reduction in cycling stability is closely related to the formation of more condensed structures during the continuous process of water loss.

Acknowledgements

This work was partially supported by the National Natural Science Foundation of China (20633040 and 20925312), the State Key Basic Research Program of PRC (2007CB209703), and Shanghai Science & Technology Committee (09XD1400300, 08DZ2270500).

References

[1] Szilvia Papp, László Kõrösia, Vera Meynen, Pegie Cool, E.F. Vansant, I. Dékány, J. Solid State Chem. 178 (2005) 1614.
[2] E. Morgado Jr., P.M. Jardim, B.A. Marinkovic, F.C. Rizzo, M.A.S. de Abreu1, J.L. Zotin, A.S. Araújo, Nanotechnology 18 (2007) 495710.
[3] S. Zhang, Q. Chen, L.-M. Peng, Phys. Rev. B 71 (2005) 014104.
[4] K.R. Zhu, Solid State Commun. 144 (2007) 450.
[5] L.M. Torres-Martínez, I. Juárez-Ramírez, K.D. Ángel-Sánchez, L. Garza-Tovar, A. Cruz-López, G. Del Ángel, J. Sol–Gel Sci. Technol. 47 (2008) 158.
[6] H.Y. Zhu, X.P. Gao, Y. Lan, D.Y. Song, Y.X. Xi, J.C. Zhao, J. Am. Chem. Soc. 126 (2004) 8380.
[7] A. Riss, J. Am. Chem. Soc. 131 (2009) 6198.
[8] H. Zhang, G.R. Li, L.P. An, T.Y. An, X.P. Gao, H.Y. Zhu, J. Phys. Chem. C 111 (2007) 6143.
[9] J.R. Li, Z.L. Tang, Z.T. Zhang, Chem. Mater. 17 (2005) 5848.
[10] M. Wei, K. Wei, M. Ichihara, H. Zhou, Electrochem. Commun. 10 (2008) 1164.
[11] J.R. Li, Z.L. Tang, Z.T. Zhang, Electrochem. Commun. 7 (2005) 62.
[12] A. Armstrong, G. Armstrong, J. Canales, R. García, P. Bruce, Adv. Mater. 17 (2005) 862.
[13] A.R. Armstrong, G. Armstrong, J. Canales, P.G. Bruce, Angew. Chem. Int. Ed. 43 (2004) 2286.
[14] R. Yoshida, Y. Suzuki, S. Yoshikawa, J. Solid State Chem. 178 (2005) 2179.
[15] Y. Suzuki, S. Yoshikawa, J. Mater. Res. 19 (2004) 982.
[16] Z. Ogumi, M. Inaba, Bull. Chem. Soc. Jpn. 71 (1998) 521.
[17] G. Armstrong, A.R. Armstrong, J. Canales, P.G. Bruce, Electrochem. Solid-State Lett. 9 (2006) A139.
[18] M. Inaba, Y. Oba, F. Niina, J. Power Sources 189 (2009) 580.
[19] H. Izawa, S. Kikkawa, M. Koizumi, J. Phys. Chem. 86 (1982) 5023.
[20] T.P. Feist, P.K. Davies, J. Solid State Chem. 101 (1992) 275.
[21] M. Casarin, A. Vittadini, A. Selloni, ACS Nano 3 (2009) 317.
[22] B.G. Hyde, Solid State Sci. 5 (2003) 15.
[23] A.D. Wadsley, S. Andersson, Acta Crystallogr. 15 (1962) 194.
[24] P.G. Bruce, B. Scrosati, J.-M. Tarascon, Angew. Chem. Int. Ed. 47 (2008) 2930.